ELSEVIER

Physica D 105 (1997) 207–225

PHYSICA D

Spirals in excitable Media. II: Meandering transition in the diffusive free-boundary limit

David A. Kessler [a], Raz Kupferman [b,*]

[a] *Minerva Center and Department of Physics, Bar-Ilan University, Ramat-Gan 52900, Israel*
[b] *Lawrence Berkeley National Laboratory, 50A-2152, 1 Cyclotron Road, Berkeley, CA 94720, USA*

Received 1 July 1996; revised 16 October 1996; accepted 17 October 1996
Communicated by L. Kramer

Abstract

In this paper we present a numerical stability calculation for steadily rotating spirals in an excitable medium. While experiments, as well as numerical simulations of two-field reaction–diffusion models have shown the existence of a Hopf bifurcation from steady rotations to a meandering state, all the analytical approaches so far have failed to predict this transition. This mismatch between analysis and simulations raises the question whether meandering critically depends on the finite diffusivity of the interface separating between the excited and the refractory phases. Our calculations show that this is not the case. The meandering transition takes place even in the limit of an infinitely sharp interface. The boundaries of the meandering transition as function of the model parameters are traced. We discuss possible explanations for the failure of previous analytical approaches.

1. Introduction

The study of spiral patterns in excitable media has been the focus of considerable attention in recent years (for a review, see [1]). Much progress has been achieved in this area through the use of simulations [2–4], the analysis of various limiting cases [5–8], and most recently, the numerical solution of the steady state problem [9–11]. Spirals are relevant not only in the context of chemical reactions, such as the famed Belousov–Zhabotinskii reaction [12,13], but also in various biological systems, such as electrical conduction in heart tissue [14], and aggregation of the slime mold [15].

Spirals exhibit a wide range of interesting dynamics. In particular, simulations reveal a Hopf bifurcation from steady-state rotation to meandering as some of the control parameters are varied. In the steady state, the spiral tip rotates at constant frequency about some fixed point. In contrast, the meandering state is a compound rotation where the distance of the tip to the center of rotation oscillates periodically. By simulating the model near the transition point, Barkley [2] and Karma [3] were able to demonstrate the Hopf nature of the transition and calculate

* Corresponding author. E-mail: raz@mekong.lbl.gov.

PII S0167-2789(96)00298-9

the unstable eigenmode. Subsequently, Barkley [9] directly demonstrated the Hopf nature of the bifurcation from a numerical stability analysis.

There remain, however, many open questions regarding this transition to meandering. In particular, the analytical treatments to date [6,7,16] have failed to reveal the existence of this bifurcation. The connection between the numerical results and analysis is obscured by the fact that the analysis is restricted to the thin-interface limit. The calculations to date, however, were done in the context of the two-field model, and thus restricted to not-too-small values of ϵ. [1]

This thin-interface, or free-boundary, limit arises [18] from taking the ratio $1/\epsilon$ of the reaction rates of the bi-stable reaction to the refractory reaction to be large. In this limit, the dynamics reduces to that of the single "slow" field. The spiral can then be considered as a sharp interface between two different phases of the fast field, the so-called "excited" and "refractory" regions. One very useful outcome of the thin-interface limit is that the spiral achieves a simple scaling form, known as Fife scaling [19]. In this form, the parameter ϵ only determines the overall length and time scales of the pattern.

Another crucial assumption needed for the analytical treatment is the smallness of the diffusion constant D of the slow field. When D is small, the diffusion of v can be ignored everywhere outside a small region around the spiral tip. It is possible then to construct a solution for this so-called "outer" region that leads to the selection of a unique rotation frequency. The outer solution, however, has an unphysical behavior at the tip. This can be resolved by rescaling space near the tip, and the construction of a solution for this core region, which has to be matched to the outer solution [6,20]. The analysis [7,21] indicates that the interesting stability properties arise from the core region. A stability analysis [7] about the core solution yielded a *real* unstable mode, as opposed to the complex conjugate modes of a Hopf bifurcation. It is unclear how to reconcile these results to the simulation results discussed above. One possibility is that the meandering transition critically depends on the finite diffusivity of the interface (a finite-ϵ effect). It is crucial, therefore, to examine the question of whether the thin-interface and weak diffusion limits preserve the generic features of spiral dynamics, including the meandering transition, or alternatively induce new features not seen for finite thickness interfaces.

In this paper we present a numerical stability calculation of spirals in the free-boundary limit. This calculation is performed for a perturbation about the steady-state free-boundary spirals numerically constructed in [11]. The method is based on the idea [10,11] of mapping the spiral interface to the x-axis so that the excited (refractory) region maps onto the upper (lower) half-plane.

Our major finding is that the free-boundary spiral indeed undergoes a Hopf bifurcation, that is, the free-boundary limit does preserve the meandering transition. We trace out the meandering transition point as a function of the various parameters. In general, the instability is enhanced for large asymmetry between the two phases (or a low excitability threshold), and for small value of D. Small values of ϵ generally tend to stabilize the solution. We find that there is a subtle interplay between the small ϵ and D limits. The results crucially depend on the relative sizes of these two small quantities. For intermediate values of ϵ, the stability properties as a function of D may even be nonmonotonic. Specifically, for decreasing D, the initial instability may be followed by a re-entrance into the stable regime before destabilizing again. We also compare our results to those of Barkley [9] for the two-field spiral stability at $D = 0$.

2. The model

We start from the two-variable reaction–diffusion system studied by Barkley [2],

$$\dot{u} = \nabla^2 u + \frac{1}{\epsilon} u(1-u)\left(u - \frac{v+b}{a}\right), \tag{1a}$$

[1] Note, however, the very recent work in [17], which simulates the thin-interface limit directly. We discuss this in the conclusions.

$$\dot{v} = D\nabla^2 v + u - v. \tag{1b}$$

The fast variable u, by virtue of the smallness of ϵ, is always either 0 (refractory, "−") or 1 (excited, "+"), except for sharp transition regions of width $\sqrt{\epsilon}$. Thus, the u-field can be eliminated, resulting in the v-field dynamics,

$$\dot{v}_+ = D\nabla^2 v_+ + 1 - v_+, \tag{2a}$$

$$\dot{v}_- = D\nabla^2 v_- - v_-, \tag{2b}$$

in the two phases, respectively. The v-field is continuous and has continuous first derivatives across the transition regions, or interfaces. The dynamics of these interfaces is given by the eikonal equation,

$$c_n = -\kappa + \frac{\nu(v_{int})}{\sqrt{\epsilon}}, \tag{3}$$

whereby the normal velocity c_n of a given point on the interface is given by the interfacial curvature κ and the value of v at this point. We adopt the sign convention that the interface has positive velocity if the excited phase propagates into the refractory phase. Similarly, the interface curvature is positive when the excited region is convex. The function ν can be computed from an analysis of soliton propagation in Eq. (1a). For our purposes, it is sufficient to replace ν by its linear expansion around the stall value $v_s = \frac{1}{2}a - b$, where ν vanishes, so that

$$\nu(v_{int}) = -\frac{\sqrt{2}}{a}(v_{int} - v_s). \tag{4}$$

As the constant a can be eliminated (in this limit) by an appropriate redefinition of ϵ, we will for convenience set $a = 1$. It is also convenient at this point to shift the v-field by the constant v_s, yielding the equations

$$\dot{v} = D\nabla^2 v - v + g_\pm, \tag{5a}$$

$$c_n = -\kappa - \frac{\sqrt{2}}{\sqrt{\epsilon}} v_{int}, \tag{5b}$$

where $g_+ = 1 - v_s$ and $g_- = -v_s$.

At this point, it is relevant to mention the Fife scaling obtained by the transformation $x \to \epsilon^{1/6}x$, $t \to \epsilon^{1/3}t$, and $v \to \epsilon^{1/3}v$. Eq. (2) then reads

$$\dot{v} = D\nabla^2 v - \epsilon^{1/3} v + g_\pm, \tag{6a}$$

$$c_n = -\kappa - \sqrt{2} v_{int}. \tag{6b}$$

Thus, the parameter ϵ appears only in the "mass" term as a coefficient of v in the diffusion equation. This mass is formally of order $\epsilon^{1/3}$. As we will see, this term plays a crucial role in the dynamics of the spiral, and we therefore choose not to drop it, continuing instead to analyze the system equation (2).

We are interested in analyzing the stability of steady-state spiral shapes which are rigidly rotating at frequency ω. The steady-state spiral consists of a "front", along which the excited phase invades the refractory phase, and a "back" along which the system reverts to the refractory state. The front and back meet at the spiral tip, where c_n vanishes, at a distance r_t from the rotation center fixed at the origin. The ray connecting the center of rotation to the tip makes an angle θ_t with the x-axis. Going into the co-rotating frame, our equations read in the polar (r, θ) coordinates,

$$\dot{v} = D\nabla^2 v + \omega \frac{\partial v}{\partial \theta} - v + g_\pm, \tag{7a}$$

$$c_n = -\kappa - \frac{\sqrt{2}}{\sqrt{\epsilon}} v_{int}. \tag{7b}$$

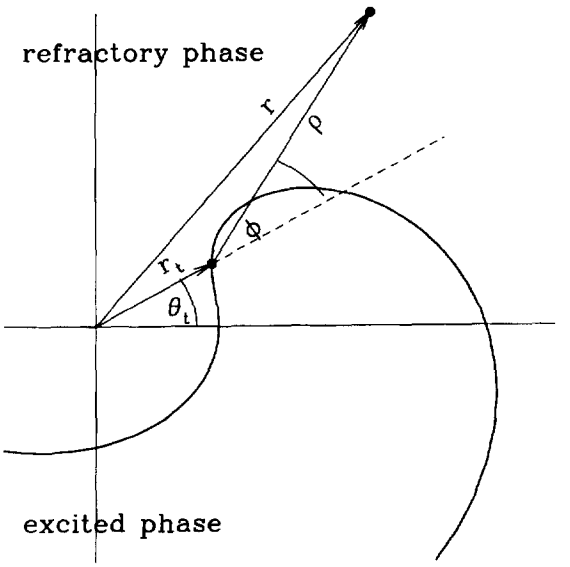

Fig. 1. Schematic plot of the spiral geometry. In the fixed (r, θ) coordinates, the origin coincides with the center of rotation. The interfaces are parametrized by $\theta_f(r, t)$ and $\theta_b(r, t)$. The transformed (ρ, φ) coordinates are centered at the spiral tip, which is defined as the point of closest approach of the spiral to the fixed origin. The new system is oriented such that the $\varphi = 0$ direction is along the ray connecting the fixed origin to the tip.

When discussing the time-dependent perturbations about the steady state, we need to define what we mean by the "tip". We take the time-dependent tip position $(r_t(t), \theta_t(t))$ in the comoving frame defined above to be the point of closest approach of the spiral to the origin in this frame. This clearly reduces to our previous definition of the tip in the steady-state problem. Then the spiral position can be parametrized by the functions $\theta_f(r, t)$ and $\theta_b(r, t)$, which are defined for $r \geq r_t(t)$.

The core of the difficulty when numerically treating the diffusion equation (7a) is the discontinuity of the operators along the yet unknown interfaces. Moreover, the eikonal equation refers to values of v along the interfaces, which do not necessarily pass through the grid points. This two obstacles can be eliminated as follows. The idea, due to Keener [10], is to transform the plane so that the excited (refractory) region maps onto the lower (upper) half-plane. The spiral front and back map accordingly onto the positive and negative x-axes in the new coordinate system.

We first transform to a polar coordinate system (ρ, φ) centered at the spiral tip. We orient the axes such that the $\varphi = 0$ direction is parallel to the ray connecting the fixed origin to the tip (Fig. 1). The transformation from (r, θ) to (ρ, φ) is in general time-dependent, and is given by

$$r\cos\theta = r_t(t)\cos\theta_t(t) + \rho\cos[\varphi + \theta_t(t)], \qquad r\sin\theta = r_t(t)\sin\theta_t(t) + \rho\sin[\varphi + \theta_t(t)]. \tag{8}$$

In this new coordinate system, the front and the back are given by new functions $\varphi_f(\rho, t)$ and $\varphi_b(\rho, t)$, with

$$\varphi_f(0, t) = \tfrac{1}{2}\pi, \qquad \varphi_b(0, t) = \tfrac{3}{2}\pi \tag{9}$$

at the tip.

Next, we map the (ρ, φ) plane onto new polar coordinates, (ρ, α). The transformation assumes that the positions of the spiral front and back, $\varphi_f(\rho, t)$ and $\varphi_b(\rho, t)$ are known. The new angular coordinate, α, is implicitly defined by

$$\varphi \equiv \alpha + \varphi_f(\rho, t) + [\varphi_b(\rho, t) - \varphi_f(\rho, t) - \pi]\sin^2\tfrac{1}{2}\alpha. \tag{10}$$

It is easily verified that the front $\varphi = \varphi_f(\rho, t)$ maps now to the ray $\alpha = 0$ (the positive x-axis), whereas the back $\varphi = \varphi_b(\rho, t)$ maps to the ray $\alpha = \pi$ (the negative x-axis).

The diffusion equation (7a) needs to be written in terms of the new (ρ, α, t) coordinates. For that, we will need the following derivatives of the mappings:

$$\dot{\rho} \equiv \left(\frac{\partial \rho}{\partial t}\right)_{r,\theta} = -\dot{r}_t \cos\varphi - r_t \dot{\theta}_t \sin\varphi,$$

$$\dot{\varphi} \equiv \left(\frac{\partial \varphi}{\partial t}\right)_{r,\theta} = -\dot{\theta}_t + \frac{\dot{r}_t}{\rho} \sin\varphi - \frac{r_t}{\rho}\dot{\theta}_t \cos\varphi,$$

$$\dot{\alpha} \equiv \left(\frac{\partial \alpha}{\partial t}\right)_{\rho,\phi} - \frac{\dot{\varphi}_f + (\dot{\varphi}_f - \dot{\varphi}_b)\sin^2(\alpha/2)}{1 + (1/2)(\varphi_b - \varphi_f - \pi)\sin\alpha},$$

$$g_1 \equiv \left(\frac{\partial \alpha}{\partial \rho}\right)_{\varphi,t} = -\frac{\varphi_f' + (\varphi_b' - \varphi_f')\sin^2(\alpha/2)}{1 + (1/2)(\varphi_b - \varphi_f - \pi)\sin\alpha},$$

$$g_2 \equiv \left(\frac{\partial \alpha}{\partial \varphi}\right)_{\rho,t} = \frac{1}{1 + (1/2)(\varphi_b - \varphi_f - \pi)\sin\alpha},$$

$$g_3 \equiv \left(\frac{\partial g_2}{\partial \alpha}\right)_{\rho,t} = -\frac{(1/2)(\varphi_b - \varphi_f - \pi)\cos\alpha}{\{1 + (1/2)(\varphi_b - \varphi_f - \pi)\sin\alpha\}^2},$$

$$g_4 \equiv \left(\frac{\partial g_1}{\partial \rho}\right)_{\alpha,t} = -g_2\left\{\left[\varphi_f'' + (\varphi_b'' - \varphi_f'')\sin^2\frac{\alpha}{z}\right] + \frac{g_1}{2}(\varphi_b' - \varphi_f')\sin\alpha\right\},$$

$$g_5 \equiv \left(\frac{\partial g_1}{\partial \alpha}\right)_{\rho,t} = -\frac{g_2}{2}\{(\varphi_b' - \varphi_f')\sin\alpha + g_1(\varphi_b - \varphi_f - \pi)\cos\alpha\},$$

where dots denote time derivatives, and primes stand for derivatives with respect to ρ

The transformed diffusion equation now reads

$$\begin{aligned}\frac{\partial v}{\partial t} + h_1(\rho,\alpha,t)\frac{\partial v}{\partial \alpha} + h_2(\rho,\alpha,t)\frac{\partial v}{\partial \rho} \\ = D\left[\frac{\partial^2 v}{\partial \rho^2} + \frac{1}{\rho}\frac{\partial v}{\partial \rho} + f_1(\rho,\alpha,t)\frac{\partial^2 v}{\partial \alpha^2} + f_2(\rho,\alpha,t)\frac{\partial v}{\partial \alpha} + f_3(\rho,\alpha,t)\frac{\partial^2 v}{\partial \alpha\,\partial \rho}\right] \\ + \omega\left[f_4(\rho,\alpha,t)\frac{\partial v}{\partial \rho} + f_5(\rho,\alpha,t)\frac{\partial v}{\partial \alpha}\right] - v + g_{\pm},\end{aligned} \tag{11}$$

where the coefficient functions $h_i(\rho, \alpha, t)$ and $f_i(\rho, \alpha, t)$ are given by

$$h_1 = \dot{\alpha} + g_1\dot{\rho} + g_2\dot{\varphi}, \qquad h_2 = \dot{\rho},$$

$$f_1 = g_1^2 + \frac{g_2^2}{\rho^2}, \qquad f_2 = g_4 + g_1 g_5 + \frac{g_1}{\rho} + \frac{g_2 g_3}{\rho^2}, \qquad f_3 = 2g_1,$$

$$f_4 = r_t \sin\varphi, \qquad f_5 = r_t \sin\varphi\, g_1 + \left(1 + \frac{r_t}{\rho}\cos\varphi\right) g_2.$$

The eikonal equation is expressed in terms of the interface position, $\varphi_{f,b}(\rho, t)$. The normal velocity c_n is given by

$$c_n = \pm\frac{\rho(\omega + \dot{\varphi}_{f,b} + \dot{\theta}_t) + r_t(\omega + \dot{\theta}_t)(\cos\varphi_{f,b} - \rho\varphi_{f,b}'\sin\varphi_{f,b}) - \dot{r}_t(\sin\varphi_{f,b} + \rho\varphi_{f,b}'\cos\varphi_{f,b})}{[1 + (\rho\varphi_{f,b}')^2]^{1/2}}, \tag{12}$$

and the curvature κ by

$$\kappa = \pm \frac{-\rho^2(\varphi'_{\mathrm{f,b}})^3 - \rho\varphi''_{\mathrm{f,b}} - 2\varphi'_{\mathrm{f,b}}}{[1 + (\rho\varphi'_{\mathrm{f,b}})^2]^{3/2}}, \tag{13}$$

where the "+" ("−") refers to the front (back).

Special attention is required in treating the diffusion equation (11) at the origin, as parts of the coefficient functions h_i and f_i diverge for $\rho \to 0$. For small values of ρ, the v-field can be expanded as

$$\begin{aligned} v(\rho, \alpha, t) \sim\ & a_0(t) + a_{1c}(t)\rho\, \cos\alpha + a_{1s}(t)\rho\, \sin\alpha \\ & + a^{\pm}_{20}(t) + a^{\pm}_{2c}(t)\rho^2\, \cos 2\alpha + a^{\pm}_{2s}(t)\rho^2\, \sin 2\alpha + \mathrm{O}(\rho^3), \end{aligned} \tag{14}$$

where the $a_i^{\pm}$ refer to the excited and refractory regions, respectively. The expansion coefficients above first-order differ between the two domains as a result of the discontinuity of the second derivative of the v-field across the interfaces. Substitution of expansion (14) into Eq. (11) along with an averaging over the angular coordinate α gives

$$\dot{a}_0 + \dot{r}_t\, a_{1s} + r_t\theta_t\, a_{1c} = D[a^{+}_{20} + a^{-}_{20} - 2\varphi'_{\mathrm{f}}(0)\, a_{1s}] + \omega r_t\, a_{1c} - a_0 + \tfrac{1}{2}(g_+ + g_-). \tag{15}$$

3. The numerical procedure

3.1. Steady-state spirals

For steady-state spirals the time-derivatives vanish, and Eqs. (11)–(13) reduce to the system studied in [11]. Note that the system is rotationally invariant, hence we may arbitrarily fix the angular orientation of the spiral, the natural choice being to locate the tip on the x-axis by setting $\theta_t = 0$.

The solution is calculated as follows: Given trial interface curves $\varphi_{\mathrm{f}}(\rho)$ and $\varphi_{\mathrm{b}}(\rho)$, along with values for ω and r_t, we can calculate the field $v_{\mathrm{int}}(\rho)$ along the interfaces in two independent ways. The first is by solving the reaction–diffusion equation (11). The second is via the eikonal equation, as $v_{\mathrm{int}}(\rho)$ is determined from the interface curves through κ and c_{n}. In order to have a consistent solution, we have to find values of $\varphi_{\mathrm{f}}(\rho)$, $\varphi_{\mathrm{b}}(\rho)$, ω, and r_t such that the two calculations of v_{int} agree for all ρ. Thus, if we have a mesh of $N+1$ points in ρ ($\rho_i, i = 0, \ldots, N$), we have $2N$ nonlinear equations ($2N-2$ matching equations for v_{int} in the interior, one at the tip, and the smoothness condition $\varphi'_{\mathrm{f}}(0) = -\varphi'_{\mathrm{b}}(0)$) for the $2N$ variables ($N-1$ interior values for each of φ_{f} and φ_{b}, ω and r_t). These equations are then solved by means of a Newton's method solver, starting from some initial guess.

Several technical points are worth further discussion. The coefficients $a_i^{\pm}$ used to expand the v-field in the vicinity of the tip must be expressed by means of the values of the v-field at the grid points, $v(\rho_i, \alpha_j)$. This is accomplished using an appropriate interpolation scheme. For example,

$$a_{1c}(t) \approx \frac{1}{\pi(\rho_2 - \rho_1)} \sum_{j=1}^{M} \Delta\alpha_j\, \cos\alpha_j \left[\frac{\rho_2}{\rho_1} v(\rho_1, \alpha_j, t) - \frac{\rho_1}{\rho_2} v(\rho_2, \alpha_j, t)\right], \tag{16}$$

up to correction terms of $\mathrm{O}(\Delta\rho^2)$.

We also need to specify boundary conditions for our solutions of both the diffusion and eikonal equations. The diffusion equation is solved on the finite interval $\rho \in (0, \rho_{\max})$, when $\rho_{\max}$ is chosen sufficiently large so that the spiral completes one turn. In [11], we used no-flux boundary conditions, requiring $\partial v/\partial\rho = 0$ at $\rho_{\max}$. Accordingly, we required φ'_{f} and φ'_{b} to vanish at the outer boundary for the eikonal equation. This arbitrary choice of boundary conditions was considered harmless as all the quantities of interest proved to be insensitive to the boundaries. To

study the stability properties, and especially to examine the unstable modes, it was found necessary to take boundary conditions that better simulate an infinite domain.

Far from the center of rotation, the interfaces asymptotically approach Archimedean spirals,

$$\theta_{\mathrm{f,b}}(r) \sim \theta^0_{\mathrm{f,b}} - \eta r + \mathrm{O}(1/r), \tag{17}$$

where $\theta^0_{\mathrm{f,b}}$ are constants, and the pitch η is yet unknown. In terms of the (ρ, φ) coordinates, the asymptotic relationship for large ρ is

$$\varphi'_{\mathrm{f,b}}(\rho) \sim -\frac{\eta}{1 + \eta r_t \sin \varphi_{\mathrm{f,b}}}. \tag{18}$$

We used this relation as an outer boundary condition for the eikonal equation at $\rho = \rho_{\max}$. Similarly, the asymptotic behavior of the v-field satisfies

$$\frac{\partial v}{\partial r} \sim -\eta \frac{\partial v}{\partial \theta}, \tag{19}$$

which can be reformulated in terms of the (ρ, α) coordinates.

The asymptotic solution for $r \to \infty$ can be calculated by substituting relation (19) into the (r, θ) form of the diffusion equation. The v-field becomes in this limit a function only of $\theta - \theta_{\mathrm{f}}$ that satisfies

$$\eta^2 D \frac{\partial^2 v}{\partial \theta^2} + \omega \frac{\partial v}{\partial \theta} - v + g_{\pm} = 0 \tag{20}$$

with

$$v(\theta_{\mathrm{f,b}}) = \mp \frac{\sqrt{\epsilon}}{\sqrt{2}} \frac{\omega}{\eta} \tag{21}$$

at the interfaces. $v(\theta)$ is of course 2π-periodic. Eqs. (20) and (21) determine a relation between the pitch η, the frequency ω, and the angular size of the excited zone $\theta_{\mathrm{f}} - \theta_{\mathrm{b}}$.

Eq. (20) is linear, and its solution in each domain is a sum of two exponentials, $\mathrm{e}^{k_{\pm}\theta}$, with $k_{\pm} = (-\omega \pm \sqrt{\omega^2 + 4\eta^2 D})/2\eta^2 D$. For small values of D, $k_- \sim -\omega/\eta^2 D$ is large, implying the existence of a boundary layer of width $\mathrm{O}(\eta^2 D/\omega)$ on the positive-θ side of each interface. This observation is important, as the angular distribution of grid points has to be adjusted such to resolve this boundary layer. To better resolve the vicinity of the interfaces, we used a suitable reparametrization of the α coordinate. Similarly, it also proved necessary to refine the grid resolution for small values of ρ.

In principle, the relation between η and ω could be calculated numerically by solving the one-dimensional asymptotic equation. In practice, it was simpler to calculate the value of η iteratively. Starting with an arbitrary guess for η, we calculated the steady-state solutions (20) and (21), and used it in turn to evaluate the asymptotic value of $\theta'_{\mathrm{f,b}}(r)$. Such a procedure was found to converge extremely quickly.

3.2. The stability calculation

We now describe the procedure for calculating the stability spectrum of a given steady-state spiral. In general, an arbitrary perturbation consists of a rigid translation, a rigid rotation, and a deformation. In terms of the (ρ, φ, t) parametrization, such general perturbations can be expanded in Fourier modes of the form

$$\varphi_{\mathrm{f,b}}(\rho, t) = \varphi^0_{\mathrm{f,b}}(\rho) + \delta\varphi_{\mathrm{f,b}}(\rho)\, \mathrm{e}^{\Omega t}, \tag{22}$$

$$r_t(t) = r_t^0 + \delta r_t\, \mathrm{e}^{\Omega t}, \tag{23}$$

$$\theta_t(t) = \delta\theta_t \, e^{\Omega t}. \tag{24}$$

(The superscript 0 denotes the unperturbed stationary solution.)

A perturbation in the position of the interfaces induces in turn a perturbation in the v-field. In particular, the value of the v-field along the interfaces, $\delta v_{\rm int}(\rho, t)$, is going to change, both due to the change in the field and due to the shift of the interfaces. The case is now similar to that encountered in the steady-state calculation. For any given perturbation of the interfaces, $\delta v_{\rm int}(\rho, t)$ can be calculated in two independent ways; from the (linearized) diffusion and eikonal equations.

For an $N+1$ point mesh in ρ, the perturbation consists of $2N-1$ degrees of freedom. These are δr_t, $\delta\theta_t$, and $2N-3$ values of $\delta\varphi_{\rm f,b}$. Three of the $2N$ interior points are determined by the condition that $\delta\varphi_{\rm f}(0) = \delta\varphi_{\rm b}(0) = 0$ at the tip, and by the smoothness condition, $\delta\varphi'_{\rm f}(0) = -\delta\varphi'_{\rm b}(0)$. These $2N-1$ unknowns are balanced by an equal number of matching equations for $\delta v_{\rm int}$ at the $2N-2$ interior points, and at the tip. This time the condition for having a consistent solution constitutes a generalized eigenvalue equation for the amplification rate of the perturbation Ω.

Consider first the reaction–diffusion equation. The coefficient functions, h_i, by virtue of being time derivatives, are first order in the perturbation. The functions f_i, on the other hand, can be linearized with respect to the perturbation, denoting the zeroth- and first-order terms by $f_i^0 + \delta f_i \, e^{\Omega t}$. The v-field also needs to be expanded so that

$$v(\rho, \alpha, t) = v^0(\rho, \alpha) + \delta v(\rho, \alpha) \, e^{\Omega t}. \tag{25}$$

Substituting the various expansions into Eq. (11), the perturbation field, $\delta v(\rho, \alpha)$, is found to satisfy the linearized equation

$$\begin{aligned} &D\left[\frac{\partial^2\delta v}{\partial\rho^2} + \frac{1}{\rho}\frac{\partial\delta v}{\partial\rho} + f_1^0\frac{\partial^2\delta v}{\partial\alpha^2} + f_2^0\frac{\partial\delta v}{\partial\alpha} + f_3^0\frac{\partial^2\delta v}{\partial\alpha\,\partial\rho}\right] + \omega\left[f_4^0\frac{\partial\delta v}{\partial\rho} + f_5^0\frac{\partial\delta v}{\partial\alpha}\right] - (1+\Omega)\delta v \\ &\quad = h_1\frac{\partial v^0}{\partial\alpha} + h_2\frac{\partial v^0}{\partial\rho} - D\left[\delta f_1\frac{\partial^2 v^0}{\partial\alpha^2} + \delta f_2\frac{\partial v^0}{\partial\alpha} + \delta f_3\frac{\partial^2 v^0}{\partial\alpha\,\partial\rho}\right] + \omega\left[\delta f_4\frac{\partial v^0}{\partial\rho} + \delta f_5\frac{\partial v^0}{\partial\alpha}\right]. \end{aligned} \tag{26}$$

The corresponding equation at the tip is obtained by linearizing Eq. (15).

By solving Eq. (26) for δv, we obtain, in particular, the variation of v along the interfaces, δv_j. Consider the perturbation as a $(2N-1)$-element vector, Δ_i. The dependence of δv_j on Δ_i defines a linear transformation. To calculate the transformation matrix A_{ji}, we set $\Delta_i = 1$ while all the other perturbation elements are zero, and solve Eq. (26). The resulting δv_j give the coefficients A_{ji}, satisfying

$$\delta v_j = A_{ji}(\Omega)\,\Delta_i, \tag{27}$$

where we explicitly denote the dependence of the transformation matrix on Ω. This procedure has to be repeated $2N-1$ times, once for each value of i.

The eikonal equation, on the other hand, defines a direct relationship between the variation of the v-field along the interfaces and the variation of the interface curves

$$\delta v = -\frac{\sqrt{\epsilon}}{\sqrt{2}}\,\delta c_{\rm n} - \frac{\sqrt{\epsilon}}{\sqrt{2}}\,\delta\kappa. \tag{28}$$

The right-hand side can be separated into an Ω-independent term, and a term which is linearly proportional to Ω. In discrete form,

$$\delta v_j = B_{ji}\,\Delta_i + \Omega C_{ji}\,\Delta_i. \tag{29}$$

Eqs. (27) and (29) form together a generalized eigenvalue problem for the amplification rate Ω:

$$\Omega\, C_{ji}\,\Delta_i = [B_{jk} + A_{jk}(\Omega)]\,\Delta_k. \tag{30}$$

For a given trial value of Ω, the matrix product on the right-hand side is explicitly defined, and its eigenvalues, Ω_i, can be calculated. These will in general differ from Ω. One may define

$$M(\Omega) \equiv \min_i |\Omega - \Omega_i| \tag{31}$$

to be a "mismatch" function of Ω. The actual eigenvalues of the stability spectrum must satisfy $M(\Omega) = 0$. The calculation of the stability spectrum, thus, reduces to a standard root finding in the two-dimensional space of complex Ω.

4. Results

4.1. Steady-state spirals

The output of the steady-state procedure described above is well illustrated in Fig. 2. The color scale image represents the v-field. Light (dark) regions correspond to relatively large (small) values of v, that is, to the excited (refractory) phase. The blue solid line is the interface, whereas the dots mark the real space positions of the grid points used for the computation of the reaction–diffusion equation. Note how the whole grid wraps around together with the spiral interface. Also, the density of grid points is higher near the interfaces and in the vicinity of the tip.

The two phases have special symmetry properties when $g_+ = -g_- = \frac{1}{2}$. In such a case, the front and the back are just rotates of each other, meeting at the center of rotation ($r_t = 0$). This was the case originally studied by Keener [10]. For $g_+ + g_- > 0$, it is the refractory phase that in the steady-state occupies most of the plane, while a spiral wave of excitation rotates around the origin with finite tip radius. We will take $g_+ + g_-$ to be the parameter that measures the asymmetry between the two phases. Large values of $g_+ + g_-$ also imply a low excitability threshold.

A typical dependence of spiral characteristics on $g_+ + g_-$ is presented in Table 1. The rotation frequency ω decreases with increasing asymmetry. The tip radius r_t, as expected, increases with the asymmetry.

As explained above, the interesting regime of parameters is when both ϵ and D are small. This limit turns out to be very delicate, as the solution is extremely sensitive to the relative magnitude of these two parameters.

For figures see next two pages.

Fig. 2. Steady-state solution for $D = 0.2$, $\epsilon = 0.02$, and $g_+ = 0.6$. The output parameters are $r_t = 0.266$, and $\omega = 1.693$. The v-field is mapped by means of a color scale. The solid line is the interface, and the dots represent the grid points used for this calculation.

Fig. 7. The mismatch function M mapped on the complex plane of the trial eigenvalue Ω/ω for $\epsilon = 2 \times 10^{-11}$ and $D = 0.001$.

Fig. 3. Color scale map of the v-field. The blue line is the interface. The parameters are $g_+ = 0.6$, $\epsilon = 0.02$, and (a) $D = 0.2$; (b) $D = 0.01$.

Fig. 5. The mismatch function M mapped on the plane of the trial eigenvalue Ω/ω for $g_+ = 0.6$, $\epsilon = 0.02$, and (a) $D = 0.2$; (b) $D = 0.01$.

Fig. 8. Eigenvalues of the stability equation for various values of ϵ and D. Points corresponding to the same value of ϵ are connected by a solid line, whereas points corresponding to the same value of D are (optionally) connected by a black dashed line. The values of ϵ are: (a) 2×10^{-2} (red), 10^{-2} (blue), and 4.3×10^{-3} (green); (b) 1.3×10^{-3} (red), 1.6×10^{-4} (blue), and 2×10^{-11} (green). Open circles surround points with $D = 0.1$, and filled circles surround points with $D = 0.002$.

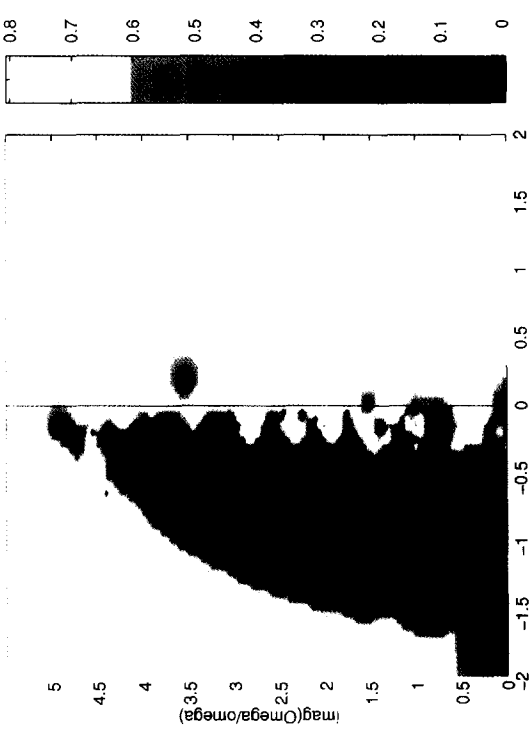

Fig. 7

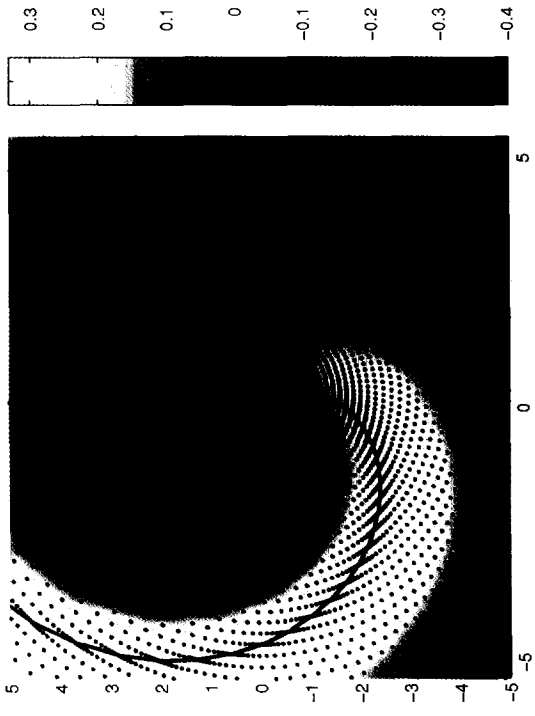

Fig. 2

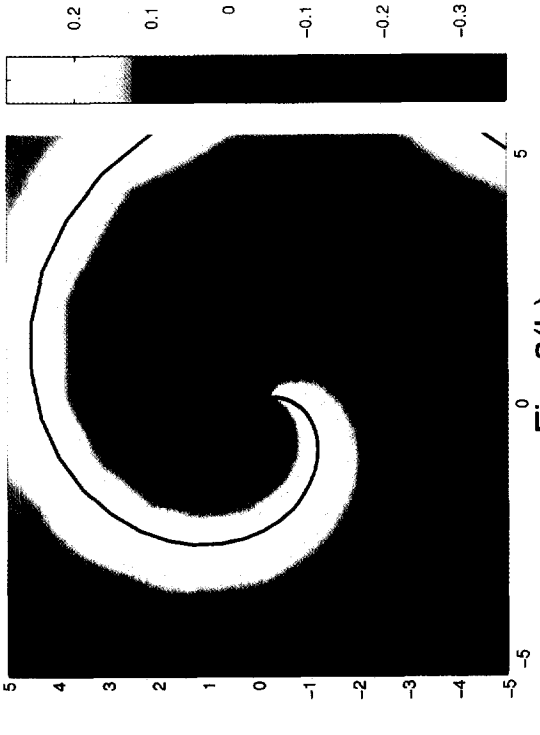

Fig. 3(b)

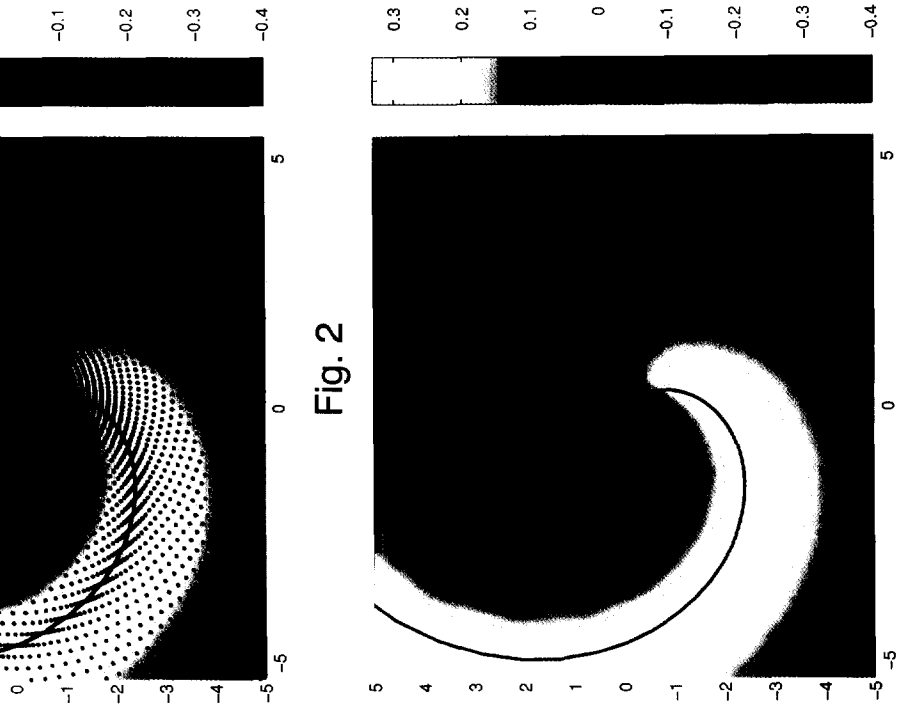

Fig. 3(a)

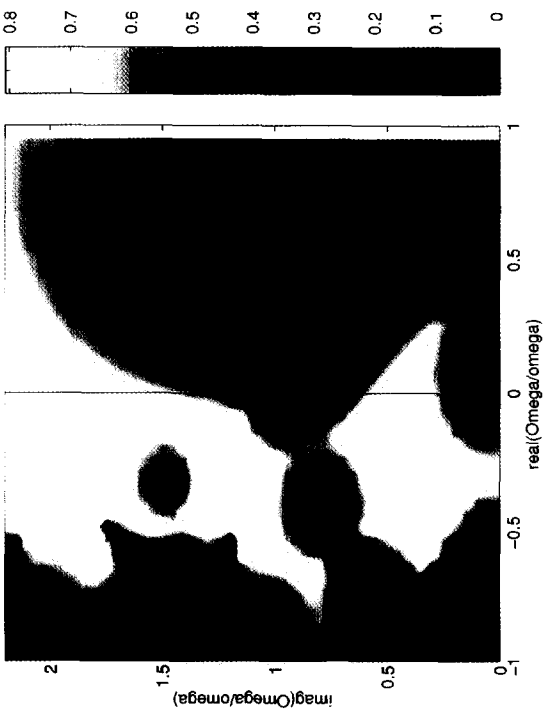

Fig. 5(b)

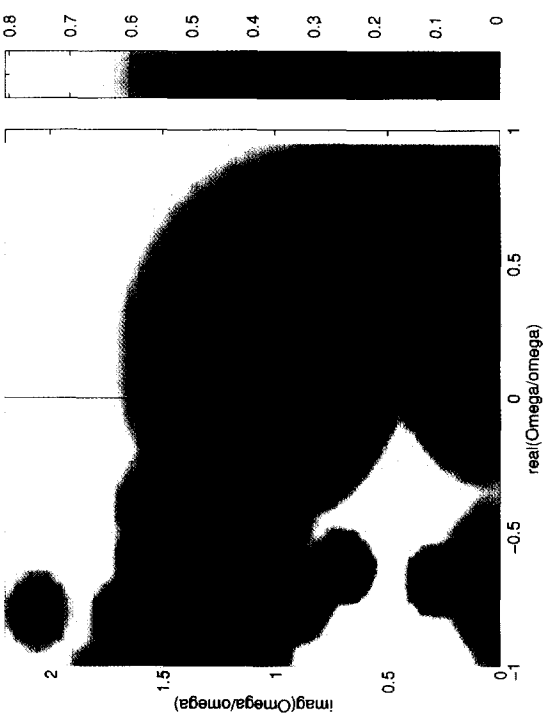

Fig. 5(a)

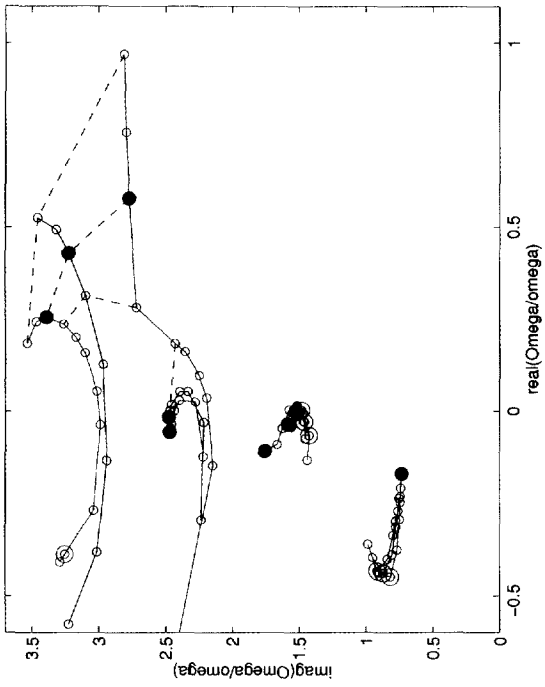

Fig. 8(b)

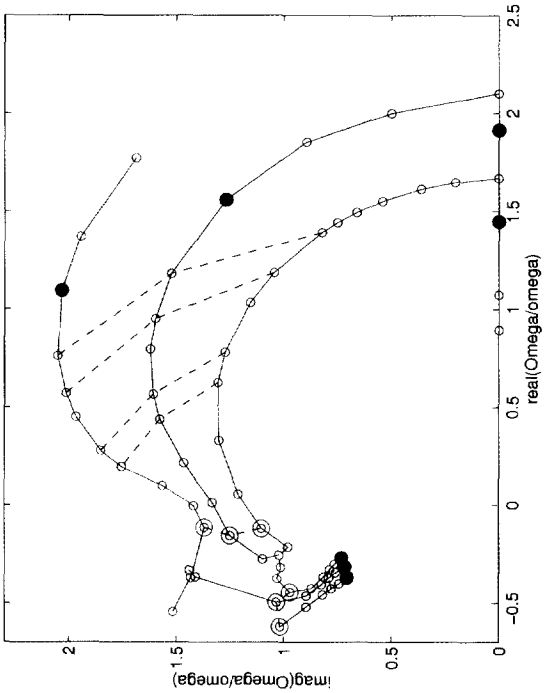

Fig. 8(a)

Table 1
Frequency, tip radius and least stable eigenvalue for varying values of the asymmetry level

$g_+ + g_-$	ω	r_t	Ω/ω
0.08	2.223	0.063	$-0.260 \pm 1.326i$
0.12	2.187	0.097	$-0.157 \pm 1.251i$
0.16	2.134	0.136	$-0.062 \pm 1.214i$
0.20	2.062	0.181	$0.025 \pm 1.174i$
0.24	1.968	0.237	$0.107 \pm 1.131i$
0.28	1.844	0.314	$0.170 \pm 1.077i$

The fixed parameters are $D = 0.05$ and $\epsilon = 0.02$.

Table 2
Rotation frequency and tip radius (in both real and Fife-scaled units), and the least stable eigenvalue for decreasing ϵ

ϵ	ω	$(\epsilon/\epsilon_0)^{1/3}\omega$	r_t	$(\epsilon/\epsilon_0)^{-1/6} r_t$	Ω/ω
1×10^{-2}	2.84	2.25	0.112	0.126	$0.060 \pm 1.373i$
2×10^{-3}	5.18	2.40	0.061	0.090	$0.013 \pm 1.491i$
2×10^{-4}	11.47	2.47	0.034	0.074	$0.002 \pm 1.524i$
2×10^{-5}	24.91	2.49	0.021	0.068	$0.004 \pm 1.530i$
2×10^{-6}	53.83	2.50	0.014	0.065	$0.005 \pm 1.531i$
2×10^{-7}	116.04	2.50	0.010	0.064	$0.006 \pm 1.532i$
2×10^{-8}	250.00	2.50	0.006	0.064	$0.007 \pm 1.532i$

The fixed parameters are $D = 0.04$, $g_+ = 0.6$, and $\epsilon_0 = 0.02$.

Table 3
Frequency, tip radius, and least stable eigenvalue as function of D

D	ω	r_t	Ω/ω	
0.0100	2.256	0.132	$0.627 \pm 1.307i$	
0.0050	2.291	0.121	$1.035 \pm 1.156i$	
0.0040	2.299	0.119	$1.187 \pm 1.044i$	
0.0030	2.307	0.117	$1.392 \pm 0.824i$	
0.0026	2.311	0.116	$1.495 \pm 0.661i$	
0.0022	2.314	0.115	$1.614 \pm 0.361i$	
0.0020	2.316	0.114	1.448	1.914
0.0015	2.320	0.112	1.074	2.673
0.0010	2.324	0.111	0.894	3.338

The fixed parameters are $g_+ = 0.6$ and $\epsilon = 0.02$.

A well-understood limit is when D is finite and $\epsilon \to 0$. The system approaches then the Fife-scaling limit. In this regime, the parameter ϵ only affects the global spatial and temporal scales of the system. Specifically, both the rotation frequency ω and the pitch η become increasingly large as $\epsilon \to 0$. Yet, by rescaling space and time, as well as the v-field by $r \to \epsilon^{1/6} r$, $t \to \epsilon^{1/3} t$, and $v \to \epsilon^{1/3} v$, the solution approaches an ϵ-independent limit. Data showing the approach of ω and r_t in Fife-scaled units to a finite limit as $\epsilon \to 0$ are presented in Table 2. The limiting value of the Fife-scaled rotation frequency ω is 2.5. This is fairly close to the theoretical expectation value of $\omega = [\sqrt{2}\pi g_+ g_- / 1.738\,(g_- - g_+)]^{2/3} = 2.66$ that holds in the limit of ϵ, $D \ll 1$.

The inverse case of finite ϵ and $D \to 0$ shows a very different behavior (see Table 3). The zero-diffusion case was previously considered by Pelce and Sun [16,21]. While their approximation successfully gives the small-D limit of the selected frequency and tip radius, its validity for studying the stability properties is questionable. The key difficulty is that the system in the zero-D limit selects a finite tip radius r_t (this value is in general a function of

ϵ, vanishing only as $\epsilon \to 0$). Thus, there is a finite "core" $r < r_t$ which entirely lies in the refractory region. In this core region, the only periodic solution for the reaction–diffusion equation,

$$\omega \frac{\partial v}{\partial \theta} - v + g_- = 0, \tag{32}$$

is the uniform solution $v = g_-$. Further analysis shows that for $r \to r_t^+$, the v-field approaches g_- linearly in $\sqrt{r - r_t}$. The $D \to 0$ limit is therefore singular, involving infinite derivatives of v all around the core circle. Of course, all these singularities are expected to be smoothed out when D is finite, but it is yet unclear how to perform a systematic perturbation expansion in small D. While the v-field develops singularities, the interface remains smooth even for $D = 0$. It is precisely the smoothness of the interface that renders the Pelce–Sun procedure suitable for calculating the steady-state solution.

Part of this behavior can be qualitatively seen in Fig. 3, where we plot a color map of the v-field for fixed ϵ and two different values of D. While for $D = 0.2$ all the equipotential lines are perfectly smooth (on the length scale of one spiral turn), they develop cusps at their inner end for $D = 0.01$. This indicates the existence of large derivatives of v in this region. Note also the unstable nature of the extreme equipotential lines along the interfaces for $D = 0.01$. This instability is a numerical artifact, which reflects our failure to adequately resolve the one-sided boundary layer. As long as this instability originates sufficiently far from the tip, it has a negligible effect on the characteristics of the steady-state solution, and on its stability properties.

This small-D behavior is substantially different than that originally studied by Bernoff [20]. For the Bernoff core solution, $r_t \sim D^{1/3} \to 0$, while the v-field remains everywhere regularly behaving. The difference arises because the Bernoff solution critically depends on the assumption that $\epsilon^{1/3} \ll D \ll 1$. Therefore, it cannot be used to predict the correct behavior for $D \to 0$ and finite ϵ.

Since most of the analytical studies of the steady-state and stability were based on the Bernoff scaling assumption, a direct comparison between our results and this limit is called for. For that, it is necessary to consider the limit where $D \to 0$, keeping $\epsilon^{1/3} \ll D$. In Table 4, we list results obtained by varying D, with $\epsilon^{1/3} = 0.1\,D$. The rotation frequency ω and the tip radius r_t are most suitably expressed in the Fife-scaled units. The Fife-scaled frequency approaches a finite limit as $D \to 0$. This matches the analytical prediction that the rotation frequency is determined for small D by the diffusionless "outer", or "far-field" solution [7]. The tip radius, on the other hand, vanishes (even in Fife-scaled units) as $D \to 0$.

The dependence of the Fife-scaled tip radius on D is plotted in Fig. 4. The points fit well to a power law

$$\left(\frac{\epsilon}{\epsilon_0}\right)^{1/6} r_t \sim D^{0.38}. \tag{33}$$

The prediction of Bernoff is a $D^{1/3}$ scaling. The deviation is perhaps due to finite ϵ effects.

Table 4
Rotation frequency and tip radius (in both real and Fife-scaled units), and the least stable eigenvalue for decreasing D

D	ϵ	ω	$(\epsilon/\epsilon_0)^{1/3}\omega$	r_t	$(\epsilon/\epsilon_0)^{-1/6} r_t$	Ω/ω
0.200	8×10^{-6}	29.33	2.161	0.0320	0.118	-0.417 ± 0.926i
0.100	1×10^{-6}	63.63	2.344	0.0173	0.090	-0.445 ± 0.831i
0.050	1.25×10^{-7}	182.14	2.472	0.0094	0.070	-0.376 ± 0.772i
0.020	8×10^{-9}	348.80	2.571	0.0042	0.049	-0.294 ± 0.753i
0.010	1×10^{-9}	708.74	2.611	0.0023	0.038	-0.246 ± 0.747i
0.005	1.25×10^{-10}	1429.41	2.633	0.0012	0.029	-0.208 ± 0.742i
0.002	8×10^{-12}	3593.90	2.648	0.0006	0.021	-0.169 ± 0.735i

The value of ϵ is varied according to the Bernoff core scaling such that $\epsilon^{1/3} = 0.1\,D$. The fixed parameters are $g_+ = 0.6$, and $\epsilon_0 = 0.02$.

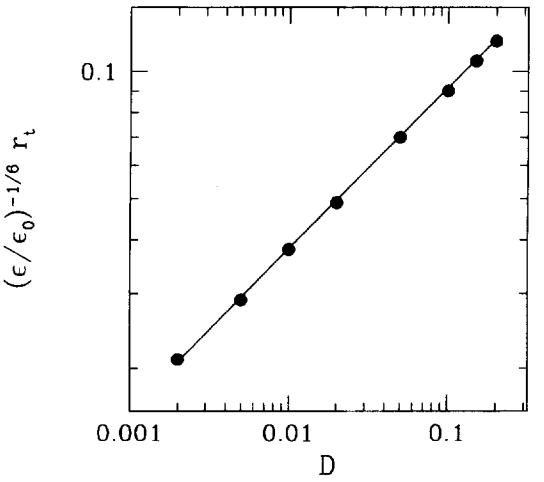

Fig. 4. Fife-scaled tip radius versus D for $g_+ = 0.6$ and $\epsilon = (0.1D)^3$.

4.2. The stability spectrum

With steady-state solutions at hand, we can now apply the stability procedure to calculate their stability spectrum. Let us first discuss those features of the spectrum dictated by symmetry considerations. The symmetries associated with the spiral solutions give rise to three "marginally stable" eigenmodes (i.e., Re $(\Omega) = 0$). One symmetry is invariance with respect to rotations about the origin. It corresponds to a real zero-mode ($\Omega = 0$) that in our parametrization is a constant angular shift in θ_t. The two other modes are a complex-conjugate pair with purely imaginary eigenvalues $\Omega = \pm i\omega$. They can be viewed as a rigid translation of the solution in the $\hat{x} \pm i\hat{y}$ directions. In terms of the (ρ, φ) parametrization, these translation modes are given by

$$\delta r_t = 1, \qquad \delta\theta_t = \pm i\frac{\kappa_t}{1 + r_t\kappa_t}\,\delta r_t, \tag{34}$$

$$\delta\varphi_{f,b}(\rho) = -\delta\theta_t \mp i\frac{\delta r_t}{1 + r_t\kappa_t}\left(\varphi'_{f,b}\sin\varphi_{f,b} - \frac{1}{\rho}\cos\varphi_{f,b}\right),$$

where κ_t is the tip curvature.

While the zero mode has a trivial representation, the imaginary translation modes have a very non-trivial form. Therefore an explicit verification that these modes satisfy the perturbation equation was used as a test for the correctness and accuracy of the procedure.

Unstable modes are characterized by $\mathrm{Re}(\Omega) > 0$. In order to perform a systematic mapping out of eigenmodes which are, or may eventually, turn unstable, we calculated the mismatch function M over a wide range of trial eigenvalues Ω (Ω being measured in terms of the natural frequency ω), on both sides of the $\mathrm{Im}(\Omega)$-axis. As complex modes always occur in conjugate pairs, it is sufficient to sweep the upper half plane. Results of this scan are shown in Fig. 5 for two different values of D. The darker regions correspond to lower values of the mismatch function, and therefore indicate the vicinity of actual eigenvalues. Note the presence of the rotational ($\Omega = 0$) and translational ($\Omega = i\omega$) modes. The density of eigenmodes was found not to change with the number of discretization grid points, indicating that all the calculated eigenmodes are discrete. For $D = 0.2$ (Fig. 5(a)), all the modes are stable, while for $D = 0.01$ (Fig. 5(b)), a pair of unstable modes is found with $\Omega/\omega = 0.627 \pm 1.307i$. The marginal

case, for which the least stable eigenvalue crosses the $\mathrm{Im}(\Omega)$-axis, occurs at some intermediate value of D, and is the threshold of the Hopf bifurcation giving rise to the meandering transition.

The next question to be addressed is how do the stability properties, and notably the transition point, vary with the parameters g_+, ϵ, and D. We start by varying the asymmetry parameter, $g_+ + g_-$. Table 1 lists the least-stable eigenvalue versus $g_+ + g_-$ for $\epsilon = 0.02$ and $D = 0.05$. The more asymmetric the two phases are, the less stable the spiral is. The bifurcation point occurs at $g_+ + g_- \approx 0.19$. Such behavior is in qualitative agreement with the results of simulations we performed using Barkley's EZ-SPIRAL program [22]. This behavior is also in qualitative agreement with the Barkley stability calculation for the two-field problem at $D = 0$. Barkley further found a restabilization of the spiral at larger g_+. Unfortunately, we are unable to probe this regime due to the limitations of our mapping to small asymmetry. This limitation can be removed by using a piecewise-linear mapping instead [23].

It is useful at this point to examine the structure of the various eigenmodes. Of particular interest is the marginally stable mode, whose structure might shed some light on the nature of the meandering transition. In Fig. 6, we compare between the imaginary parts of three different eigenmodes. The graphs in Figs. 6(a) and (b) are both eigenmodes of the marginally stable solution referred to above ($\epsilon = 0.02$, $D = 0.05$, and $g_+ = 0.595$). Fig. 6(a) shows the marginally stable mode, $\Omega = 1.18\,\mathrm{i}\omega$. Fig. 6(b) shows, for comparison, the $\Omega = \mathrm{i}\omega$ translation mode. The observation is that these two modes are very similar to each other. This similarity was already pointed out by Barkley, who furthermore found that at a certain point in parameter space the modes become degenerate, giving rise to secular behavior.

In their analytical approach, Kessler et al. [7] introduced the distinction between so-called "global" and "core" modes. The first are associated with a global perturbation, and therefore the eigenmodes $\delta\varphi(\rho)$ do not decay for large ρ. The $\Omega = \mathrm{i}\omega$ modes are examples of such global modes. Core modes, on the other hand, are associated with perturbations that are localized at the tip, and decay as ρ becomes large compared to the core radius r_t. Fig. 6(a) shows that the meandering mode remains fairly large even far from the tip. Therefore, it is hard to square this behavior with the prediction that instabilities are entirely due to core modes.

For larger values of g_+ the spiral is unstable. The unstable mode for $g_+ = 0.64$ is plotted in Fig. 6(c). This mode is relatively more localized, and mainly varies along the first half turn of the spiral. The conclusion is that the more unstable the solution is, the more the mode is localized, in accord with Barkley's findings.

The key question for comparison with the analytical theory is the behavior of the stability properties when both ϵ and D are small. To resolve this question, we fixed the value of g_+ to 0.6, and calculated eigenmodes for a wide range of values of ϵ and D. The emerging picture is rather intricate, with the stability properties critically depending on the relative magnitude of ϵ and D.

A first case to consider is when D is fixed, and $\epsilon \to 0$. As described above, ϵ may be eliminated from the equations by means of the Fife-scaling transformation. Therefore, we expect Ω/ω to approach a finite limit as $\epsilon \to 0$, like all the other (Fife-scaled) spiral characteristics. This is indeed the case, as can be seen for example in Table 2.

Next, we consider the opposite case with ϵ fixed and $D \to 0$. The generic behavior is shown in Fig. 8(a) (see also Table 3), where we follow the trajectory of the least stable modes as D is decreased. The spiral becomes increasingly less stable the smaller D is. At some critical value of D, the eigenvalue hits the real axis, and the pair of complex-conjugate modes becomes a pair of real modes. These real modes move along the real axis away from their origination point as D is further decreased.

This small D behavior is however very sensitive to the value of ϵ. The smaller ϵ is, the smaller is the critical D for which the eigenmodes turn real. Thus it is unclear whether this phenomenon has any relevance to the Bernoff regime in which $\epsilon^{1/3} \ll D \ll 1$.

The theory of Kessler et al. [7] predicts, in particular, that in the Bernoff regime all the eigenvalues have an imaginary part that is an integer multiple of ω. We checked this by mapping the mismatch function M on the complex

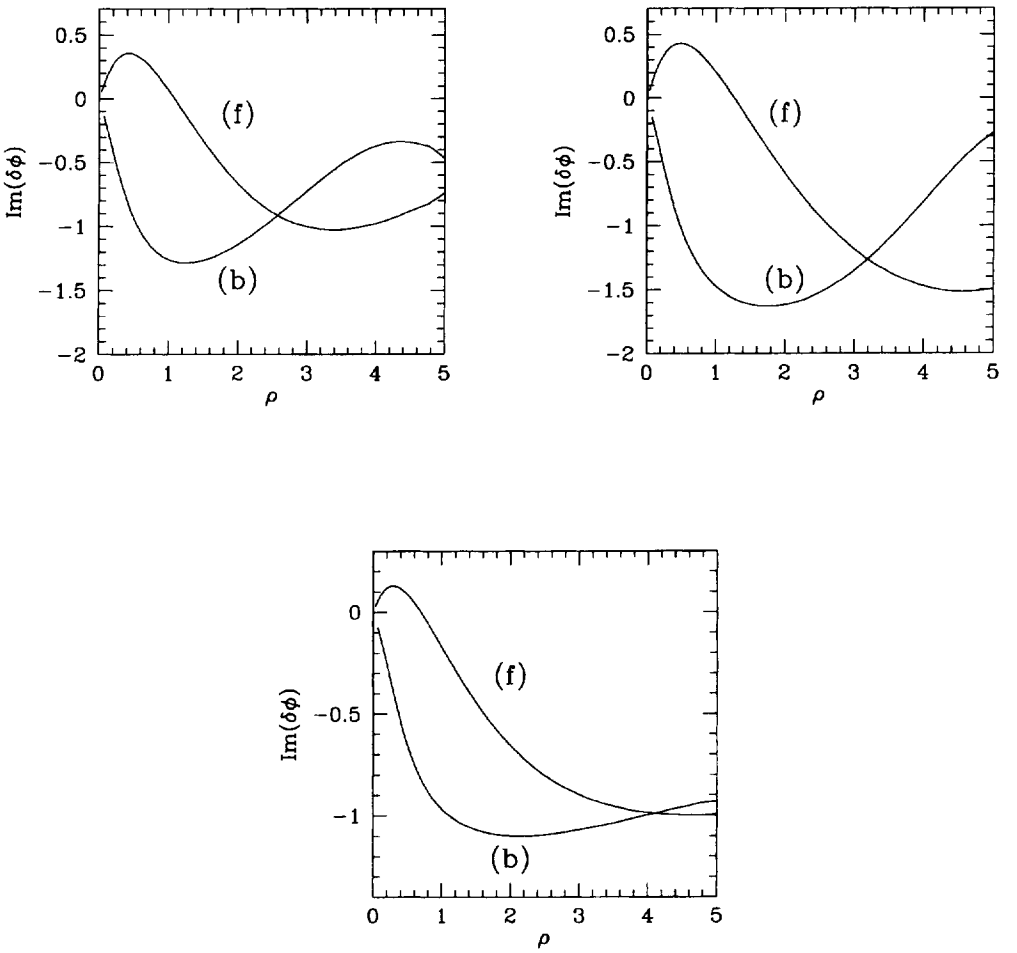

Fig. 6. The imaginary part of the eigenmode $\delta\varphi(\rho)$ for $\epsilon = 0.02$, and $D = 0.05$. The "f" ("b") refers to the front (back) curve. (a) The marginally stable mode ($\Omega = 1.18\,\mathrm{i}\omega$) for $g_+ = 0.595$. (b) The $\Omega = \mathrm{i}\omega$ translation mode for the same steady-state solution. (c) The unstable mode, $\Omega = 0.627 + 1.307\mathrm{i}$, for $g_+ = 0.64$.

plane of trial eigenvalues, Ω/ω, for $\epsilon = 2 \times 10^{-11}$ and $D = 0.001$. The result is shown in Fig. 7. Except for the real modes and the $\Omega = \mathrm{i}\omega$ translation modes, none of the other modes is found to satisfy the theoretical prediction.

To demonstrate the more subtle aspects of the crossover regimes, where both ϵ and D are finite, we plot in Fig. 8 the eigenvalues for various values of ϵ and D. Points corresponding to the same value of ϵ are connected by a solid line. Different branches of eigenvalues with the same value of ϵ have the same color. A dashed line connects between points that correspond to the same value of D.

Fig. 8(a) shows such curves for $\epsilon = 2 \times 10^{-2}$ (red), $\epsilon = 10^{-2}$ (blue), and $\epsilon = 4.3 \times 10^{-3}$ (green). For the two larger value of ϵ, we reach values of D sufficiently low so as to observe the modes turning real. Another new behavior observed here is the merging and reconnection of two branches occurring for a value of ϵ between 10^{-2} and 4.3×10^{-3}.

Subsequent curves for $\epsilon = 1.2 \times 10^{-3}$ (red), $\epsilon = 1.6 \times 10^{-4}$ (blue), and $\epsilon = 2 \times 10^{-11}$ (green) are shown in Fig. 8(b). From this succession of graphs, the following picture arises: (i) for fixed ϵ, there is only one branch that

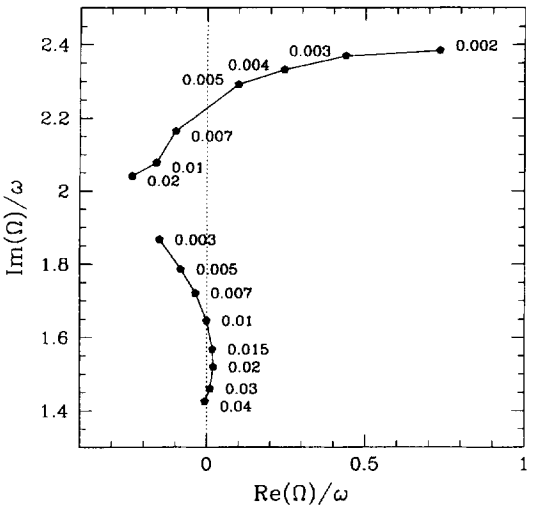

Fig. 9. "Trajectories" of the least stable eigenvalues for varying values of D. The fixed parameters are $g_+ = 0.6$ and $\epsilon = 0.0025$. The value of D appears on the plot, in the vicinity of the corresponding dot.

becomes increasingly unstable for small D. The smaller ϵ is, the smaller is the value of D for which the meandering transition occurs, and the larger is the meandering frequency at the transition point; (ii) changes in ϵ have a significant effect on the stability spectrum only if ϵ is not too small compared to D; (iii) as ϵ is decreased, the curve representing the least stable eigenvalues merges with another curve, and the two reconnect such that the new curve with the largest imaginary value becomes the least stable one. This process repeats itself as ϵ is further decreased.

This complex dependence of the stability spectrum on ϵ and D can lead to interesting stability properties. Fig. 9 shows the two least stable branches of eigenvalues for $\epsilon = 2.5 \times 10^{-3}$. For $D > 0.046$ the spiral is stable. A Hopf bifurcation to meandering occurs at this point, but the solution then re-enters into the stable zone at $D = 0.015$. A second bifurcation occurs as D is further decreased below 0.006. Thus there exists an "island" of stability for $0.006 < D < 0.015$.

5. Discussion

This paper provides a first calculation of the stability properties of steadily rotating spiral waves in the free-boundary limit. This calculation is based on an extension of the method originally proposed by Keener to map the interface onto the x-axis.

The main result of this paper is that the meandering transition is not a finite-ϵ feature, but is present also in the free-boundary limit. This finding is consistent with the recent numerical simulations of the free-boundary limit, and raises again the intriguing question as to why all former analytical studies were unable to capture this transition. Our numerical stability calculation is particularly important, as it allows for the first time to directly test the predictions of the analytical approaches.

We first compare our results to the theory of Kessler et al. [7]. This analysis is based on the Bernoff core limit where $\epsilon^{1/3} \ll D \ll 1$. Rather that a pair of complex unstable modes as we should expect, their treatment yields only a real unstable mode. Our calculation does indicate the presence of a real mode for small enough values of D,

however, it appears as if D has to be small also compared to some power of ϵ. Thus, it is not clear that this transition has any relevance to the Bernoff regime.

Another central prediction of [7] is that the eigenmodes are organized in a layered structure, all having the imaginary part of the amplification rate equal an integer multiple of the rotation frequency ω. Neither is this prediction supported by our numerical results (Fig. 7).

The imminent question is of course why does the analysis fail to predict the correct behavior? A possible weakness of the above theory is the assumption that the stability calculation can be performed by a separate consideration of the core and outer regions. Our calculations conclusively show that the bifurcation mode is far from being a core mode. This may be an indication that the approximation where the two regions of the spiral are assumed to be only weakly coupled is invalid. Such hypothesis was already suggested in [7].

Finally, our results predict that for certain ranges of parameters the stability properties as function of D may exhibit a complex behavior, whereby the meandering transition is followed (as D becomes smaller) by a re-entrance into the stable regime before destabilizing again. While this restabilization of the Hopf instability has been observed both experimentally [24] and numerically [9,25], a subsequent destabilization has yet to be observed. More work on this point is clearly needed.

Acknowledgements

Parts of this work were accomplished while R.K. was at Bell Laboratories. We thank H. Levine for many fruitful discussions. DAK thanks I. Aranson and I. Mitkov for discussions. We also thank the anonymous referee for his helpful comments. The work of DAK is supported in part by the Israel Science Foundation. RK is supported by the Applied Mathematical Sciences Subprogram of the Office of Energy Research, US Department of Energy, under Contract Number DE-AC03-76SF00098.

References

[1] E. Meron, Phys. Rep. 218 (1992) 1.
[2] D. Barkley, Phys. Rev. Lett. 68 (1992) 2090.
[3] A. Karma, Phys. Rev. Lett. 65 (1990) 2824.
[4] L. Tsimring, H. Levine and I. Aronson, Phys. Rev. Lett. 76 (1996) 1170.
[5] J.J. Tyson and J.P. Keener, Physica D 32 (1988) 327.
[6] D.A. Kessler, H. Levine and W.N. Reynolds, Phys. Rev. Lett. 68 (1992) 401.
[7] D.A. Kessler, H. Levine and W.N. Reynolds, Phys. Rev. A 46 (1992) 5264; D.A. Kessler, H. Levine and W.N. Reynolds, Physica D 70 (1994) 115.
[8] A. Karma, Phys. Rev. Lett. 68 (1992) 401.
[9] D. Barkley, Phys. Rev. Lett. 72 (1994) 164; in: Chemical waves and patterns, eds. R. Kapral and K. Showalter (Kluwer Academic, Boston, 1995).
[10] J.P. Keener, Physica D 70 (1994) 61.
[11] D.A. Kessler and R. Kupferman, Physica D 97 (1996) 509.
[12] G.S. Skinner and H.L. Swinney, Physica D 48 (1990) 1.
[13] T. Plesser, S.C. Müller and B. Hess, J. Phys. Chem. 94 (1990) 7501; J. Ross, S.C. Müller and C. Vidal, Science 240 (1988) 460.
[14] A.M. Pertsov et al., Circulation Research, 72 (1993) 631; I.R. Efimov, V.I. Krinsky and J. Jalife, Chaos, Solitons and Fractals 5 (1995) 513; A. Karma, Phys. Rev. Lett. 71 (1993) 1103.
[15] J.-L. Martiel and A. Goldbeter, Biophys. J. 52 (1987) 807; J.J. Tyson, K.A. Alexander, V.S. Manoranjan and J.D. Murray, Physica D 34 (1989) 193.
[16] P. Pelce and J. Sun, Physica D 48 (1991) 353.
[17] I. Mitkov, I. Aranson and D.A. Kessler, preprint (1996).
[18] J.P. Keener, SIAM J. Appl. Math. 46 (1986) 1039.
[19] P.C. Fife, in: Non-Equilibrium Dynamics in Chemical Systems, eds. C. Vidal and A. Pacault (Springer, New York, 1984).

[20] A.J. Bernoff, Physica D 53 (1991) 125.
[21] P. Pelce and J. Sun, Physica D 63 (1993) 353.
[22] D. Barkeley, EZ-SPIRAL, a public domain program for stimulating spiral waves, Vol. 2.
[23] Y. Portal and D.A. Kessler, in preparation.
[24] G.S. Skinner and H.L. Swinney, Physica D 48 (1991) 1.
[25] A. Winfree, Chaos 1 (1991) 303.